TRENDS IN SCIENCES 2025; 22(8): 10054
https://doi.org/10.48048/tis.2025.10054 RESEARCH ARTICLE

Growth and Characterization of Cadmium and Nickel Nanocomposites on Porous Silicon for Some Antibacterial Properties

Ghazwan Ghazi Ali[1,*], Asmaa Zaki Khalil[1] and Omar Abdulazeez Alhamd[2]

[1]*Department of Physics, College of Education for Pure Science, University of Mosul, Mosul 41002, Iraq*
[2]*Department of Biology, College of Education for Pure Sciences, University of Mosul, Mosul 41002, Iraq*

([*]Corresponding author's e-mail: dr.ghazwan39@uomosul.edu.iq)

Received: 25 February 2025, Revised: 18 March 2025, Accepted: 2 April 2025, Published: 20 June 2025

Abstract

This study uses the chemical spray technique to employ the cadmium and nickel oxide nanostructures deposited on porous silicon substrate. CdO and NiO nanocomposites were prepared by a mixture exchange process with different composites at 25 % CdO-NiO, 50 % CdO-NiO and 75 % CdO-NiO. The biological activity was studied, and it was found that the concentrations of 50 and 100 µg/mL of 50 % CdO-NiO and 75 % CdO-NiO were the best concentrations, low concentrations of the nanoparticle mixture at 25 µg/mL also encouraged the growth of symbiotic bacteria. The investigation and characterization of NiO and CdO thin films nanostructures on porous silicon at different compositions were observed. A scanning electron microscope image revealed that the particle size of the prepared samples decreased from 26.36 to 22.61 nm with an increase of Cd^{2+} content. XRD pattern showed a cubic structure and good crystallinity of CdO and NiO nanocomposites. In addition, I-V measurements refer to the presence of rectifying behavior in a hetero structure. In terms of external current, the highest value was found to be at 75 % CdO. The optical energy was decreased from 2.69 to 2.55 eV for 25 % CdO and 75 % CdO, respectively. In addition, this paper focuses on the optimization of performance mixture CdO-NiO/PSi hybrid nanostructures to enhance their physical and biological properties.

Keywords: Antibacterial, Molecular detection of bacteria, Porous silicon, CdO, NiO

Introduction

Nickel Oxide (NiO) has a wide energy gap (3.4 to 4.3 eV) and a p-type conductivity. Also, it is considered as antiferromagnetic material, and it is classified as one of the oxides of basic metals [1]. NiO is a chemical compound having a face-centered cubic (fcc) crystal structure similar to that of sodium chloride (NaCl). Nickel Oxide is a chemically stable oxide. NiO is a transparent semiconductor in the field of ultraviolet, visible and near infrared rays [2]. The cadmium oxide belongs to the TCO family group and it has a direct energy band gap of 2.6 eV. Furthermore, CdO thin film has high electric conductivity and transparency. Nickel and Cadmium oxides have many advantages in comparison with another conductive oxide in the field of commercial uses, these advantages are represented in an electrical, optical, physical and chemical properties [3], among their applications is that using in smart windows, car rearview mirrors, and high-resolution mobile display devices as an electronic paper [4]. Additionally, the optoelectronic applications have been widely used such as photodetector, filters, gas sensor and biomedical imaging [5-8]. Porous silicon nanostructure is a very important material that has been used in wide applications due to high surface area and strong photoluminescence at room temperature. This makes it suitable for a wide range of applications including light-emitting diodes, solar cells, photo detectors, chemical sensors, cancer cell imaging, biosensors, radiotherapy, and photo-radiation therapy due to the ease of modification of its surface and optical properties [9,10]. The nanocomposites of CdO-NiO could be used in numerous applications such as

biomedicine and chemical sensors due to high chemical stability. The fabrication techniques of heterojunction NiO and CdO oxides nanostructures on porous silicon are presented as an important role for the evaluation of the deposited thin films performance. In details, there are numerous procedures to prepare the NiO and CdO oxides nanostructures, which was achieved by sol-gel, chemical vapor deposition (CVD), chemical spray, chemical bath deposition, and sputtering technique [11-14]. The chemical spray technique is the easy method and it has a low cost and is not time-consuming [15,16]. The preparation methods framework of physical, chemical, and biological are characterized by treat of dyes from wastewater such as coagulation, flocculation, reverse osmosis and biological oxidation. There is a keen interest in studying the effect of nanoparticles on components of electronic and electrical devices, such as diodes and transistors, and the impact of these components on bacteria and fungi [17]. Angel *et al*. [18] prepared NiO nanocomposites in order to achieve the highest photocatalytic activity under optimal conditions in the current study. They exhibit the nanoparticles of NiO possess high chemical stability, super electron transfer capability, and anti-inflammatory properties. Anitha *et al*. [19] were studied the synthesis and characterization of NiO-CdO composite materials towards photoconductive and antibacterial applications, they exhibit NiO-CdO nanocomposite have high chemical stability, super electron transfer capability and anti-inflammatory properties. Cadmium and nickel oxides have non-toxicity and environmental friendly, as well as chemical and physical stability. This work aims to investigate the structural, electrical and optical properties of NiO-CdO on porous silicon at different weight ratio (25 % CdO-NiO, 50 % CdO-NiO and 75 % CdO-NiO) and its uses of biological applications to treat of pathogenic and rahizobium bacteria.

Materials and methods

Synthesis of porous silicon

The crystalline silicon wafer n-type with orientation (111), resistivity of 2 - 10 Ω.cm, etching time 3 min and current density of 10 mA/cm^2 were used. Firstly, the wafer Si was cleaned with alcohol and ethanol solutions by an ultrasonic bath at 10 min and rinsed with deionized water. The porous silicon was achieved using photo-electrochemical etching technique. All samples were immersed in solution containing the mixture of hydrofluoric acid (16 % HF) and ethanol (98 %). The formation scheme of porous silicon depends on the preparation conditions. Importantly, it consists of the cylinder Teflon cell shape connected with circle part 1.6 cm in order to flow the solution inside the cell. The electrical circuit was applied by 2 electrodes, The 1st one is gold mash as cathode electrode and the 2nd part is metal steel as anode electrode as **Figure 1(a)**.

Synthesis and deposition of NiO and CdO nanocomposites

The experimental procedure of nickel and cadmium nanocomposites were prepared by spray pyrolysis method. Nickel chloride ($NiCl_2{\cdot}5H_2O$) (0.74 gm, 0.1 M), particle size 10 - 30 nm and Cadmium chloride ($CdCl_2{\cdot}5H_2O$) (1.8332 gm, 0.1 M), particle size less than 20 nm were used Sigma-aldrich, 97 % purity were dissolved of each other with potassium hydroxide KOH (0.561 gm, 0.1 M) in 100 mL of distilled water with continuous stirring using a magnetic stirrer for a period of 2 h in order to obtain a homogeneous solution at a temperature of 85 °C. The different composite ratios were used such as 75 % NiO and 0.25 % CdO, 50 % NiO and 50 % CdO, 25 % NiO and 75 % CdO. Finally, all samples were deposited using chemical spray method, the parameters of fabrication conditions were applied on the glass and porous silicon surfaces at 260 °C and pressure of an atmospheric 7.5 bar, the distance between nozzle and substrate at (25 cm), the spray rate (10 mL/min) and the spray time (5 s) as **Figure 1(b)**. The solution reactions were observed using the following formula:

$$NiCl_2{\cdot}5H_2O + 2KOH \rightarrow Ni(OH)_2 + 2KCl \quad (1)$$

$$Ni(OH)_2 + 2KCl \xrightarrow{\Delta} NiO + 2KCl + H_2O\uparrow + H_2\uparrow \quad (2)$$

$$CdCl_2{\cdot}5H_2O + 2KOH \rightarrow Cd(OH)_2 + 2KCl \quad (3)$$

$$Cd(OH)_2 + 2KCl \xrightarrow{\Delta} CdO + KCl + H_2O\uparrow + H_2\uparrow \quad (4)$$

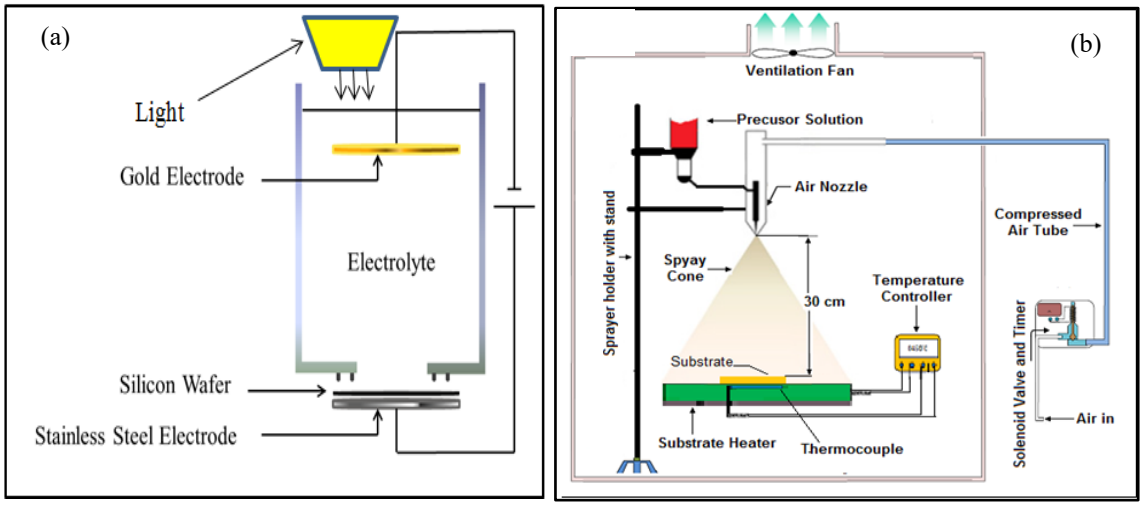

Figure 1 (a) Diagram of photo electrochemical cell and (b) Diagram of spray pyrolysis.

Chemicals and pure material

Sigma-Aldrich (Te, USA) provided the bacterial medium and the oxide nanoparticles (235673 anatases, 99.5 % trace metals base, CAS Number 1377-70-0). The *in vivo* study's reagents were purchased from scientific laboratory supplies in the United Kingdom. The culture medium was made, its pH was adjusted, and it was then autoclaved to sterilize according to the manufacturer's instructions. The media, including Mueller Hinton Agar (MHA), was acquired from Fluka, Switzerland.

Microorganisms

Different Gram-negative and Gram-positive were investigated, namely, Staphylococcus aureus, Klebsiella pneumoniae, Pseudomonas aeruginosa, Bacillus subtilis, and 4 strains of Rhizobium sp. The strain bank of the College of Education for Pure Sciences' Microbiology Department graciously identified and gave all of the strains. Rhizobium strains were obtained from the soil and were diagnosed in the laboratory. Three duplicates for each treatment were created for each treatment, and the control sample was saturated with sterile distilled water [20].

Identification of bacterial isolates

Bergey's Manual of Systematics of Each Bacteria was used to identify the chosen bacteria using morphological, cultural, and biochemical tests. The genetic sequence of the bacteria was then determined based on 16S ribosomal RNA (rRNA) gene sequencing using universal primers 27 F (5′-AAGAGT TTGATCMTGGCTCAG-3′) and 1492 R (5′-TACGGYTACCTTGTTACGACTT-3′) as a forward primer and reverse primer respectively (Eurofins Genomics Germany) were used. DNA extraction was done using the protocol of Bacterial Xpress Nucleic Acid Extraction Kit (3096 Millipore, Chemicon®). The polymerase chain reaction (PCR) product was cleaned up using the Sigma-Aldrich PCR Purification Kit (MBD0022 Sigma-Aldrich®). Agarose gel (1 %) (05066-50G Sigma-Aldrich Gillingham) was used to electrophorese the PCR product. By using the direct PCR sequencing method, the nucleotide sequence of the bacteria's 16S rRNA gene was determined by Eurofins Sanger sequencing. The cycling circumstances of PCR were according to the following: 94 °C for 10 min and 34 cycles of denaturation at 95 °C for 30 s, annealing extension at 56 °C for 1 min, 72 °C for 1 min, and an extension at 72 °C for 10 min. BLAST analysis was used to compare the 16S rRNA gene sequence with that in the NCBI GenBank database. https://www.ncbi.nlm.nih.gov/genbank/genomesubmit and cluster analysis and phylogenetic tree performed by using MEGA-X program version 10.02.06 [21].

Disk diffusion assay to estimate the influence of NPs on the viability of bacteria

The disc agar diffusion (DAD) test was used to assess the in vitro antibacterial properties of the NPs. A separate standard paper disc was further impregnated to determine NP effects with a concentration of NP (50 %, 75 % CdO-NiO). In each chosen broth medium, a

single sample strain colony was cultivated overnight on a rotary shaker (180 rpm) at 28 °C. The inoculums were created by diluting the overnight cultures and implemented to the Petri dish together with the prepared disks, that contained NP examined concentration and standard our culture collection was used as test strains. Following incubation at 37 °C for 24 h for pathogenic bacteria, and at 28 °C for 48 h for the soil bacteria, the studied bacteria were initially cultured for 1 h to serially dilution-standardize the culture to 104 CFU/mL. Twenty-five % CdO/NiO of bacteria were separated on the surface of the KBA agar plates after they had been prepared for the cultures. The sterile filter paper discs 6 mm in diameter were put on all these plates, as well as 25 µL of (25 and 50 % CdO-NiO) NPs suspended in de-ionized water were added to each filter paper disc. The inhibition zones were calculated. The tests were performed in triplicate.

Results and discussion

The spectrum analysis of XRD

Figure 2 shows the compositions of CdO-NiO/PSi at different concentrations using the XRD technique. The analysis patterns of CdO and NiO nanostructure exhibit the face-centered cubic structure (fcc). Besides, the substrate of porous silicon remains in the crystalline phase after deposition nickel and cadmium nanocomposite. Meanwhile, the peaks intensity of the CdO-NiO/PSi nanocomposites increase with an increase CdO content. Besides, the strong peak intensity of porous silicon was found to be 2θ = 27.82 ° and equal plane at (111). Apart from this, the NiO analysis at 2θ equal plane at 36.21 ° (111), 41.42 ° (200), and 61.12 ° (220) are corresponding with Card No. 67-104924. The CdO analysis at 2θ and equal plane at 31.23 ° (111), 38.2 ° (200), 51.23 ° (220), and 66.16 ° (311) corresponding with JCPDS No. 00-005-064034 [22]. The Scherrer formula was used to estimate the crystalline diameter of nanostructures, which can be given as follows:

$$L = \frac{k\lambda}{\beta\, cos\theta} \quad (5)$$

where θ is the Bragg angle, β symbolizes the full width at half maximum (FWHM), K indicates 0.912 and λ refers to the wavelength equal 0.1542 nm. The grain size reduces from 36.47 to 28.82 nm with an increase CdO due to the nature of surface structure of porous silicon during the anodization process [23].

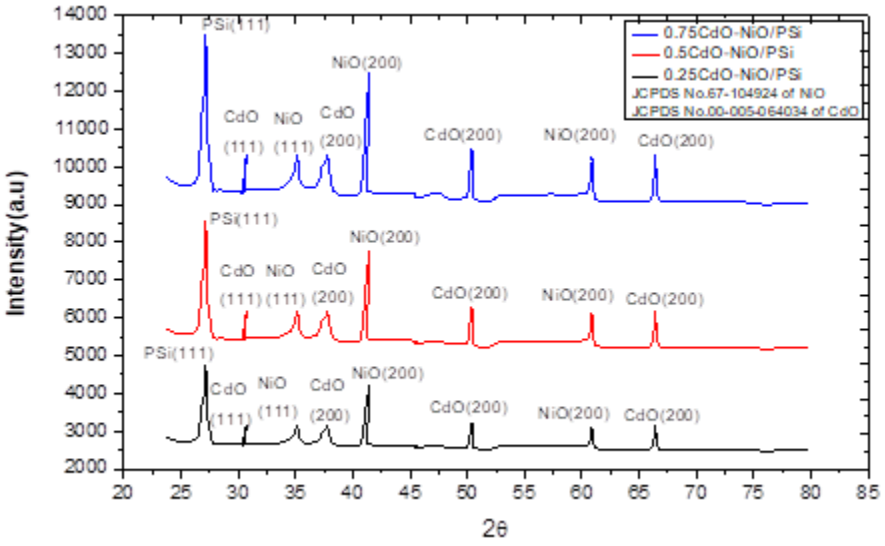

Figure 2 XRD of CdO-NiO/PSi nanocomposites deposited on porous silicon substrate at different concentration 0.25 CdO-NiO/PSi, 0.5 CdO-NiO/PSi, and 0.75 CdO-NiO/PSi.

Table 1 Data of XRD elements of CdO-NiO-PSi nanocomposites.

Sample	2θ	*hkl*	*L* (nm)	FWHM (deg)	d (A°)
0.25 CdO-NiO/PSi	27.82	111	36.47	0.541	3.221
	31.23	111	33.361	0.624	3.311
	36.21	111	31.78	0.682	3.358
	38.2	200	35.31	0.582	3.147
	41.42	200	34.62	0.636	3.245
	51.23	220	32.59	0.691	3.614
	61.12	311	33.64	0.681	3.551
	66.84	311	32.53	0.690	3.582
0.5 CdO-NiO/PSi	27.76	111	34.65	0.632	3.174
	31.21	111	31.81	0.671	3.243
	36.20	111	30.69	0.698	3.353
	38.13	200	29.62	0.727	3.482
	41.32	200	29.33	0.731	3.679
	51.11	220	29.23	0.746	3.722
	61.05	311	29.74	0.735	3.622
	66.81	311	28.56	0.814	3.735
0.75 CdO-NiO/PSi	27.76	111	34.65	0.632	3.174
	31.21	111	31.81	0.671	3.243
	36.20	111	30.69	0.698	3.353
	38.13	200	29.62	0.727	3.482
	41.32	200	29.33	0.731	3.679
	51.11	220	29.23	0.746	3.722
	61.05	311	29.74	0.735	3.622
	66.81	311	28.56	0.814	3.735

Scanning electron microscope (SEM)

The surface morphology of the CdO-NiO/PSi nanocomposites was characterized by the high-resolution micrograph (SEM). The fresh PSi has sponge like structure due to chemical dissolution during the formation period of PSi as **Figure 3(a)**. The SEM morphology of the 25 % CdO-NiO/PSi nanocomposites is shown in **Figure 3(b)**. It reveals existence of some accumulation growth of the nanoparticles at the surface. **Figure 3(c)** illustrates the surface of the 50 % CdO-NiO/PSi nanocomposites, the surface of the sample is composed of nanoscale size and uniform distribution of particles. In **Figure 3(d)**, the SEM image of the 75 % CdO-NiO/PSi nanocomposites exhibits some patches of interconnected grains and irregularly shaped due to surface morphology is primarily dominated by NiO [24]. **Figure 3(e)** and **3(f)** depicts cross section of porous silicon before and after deposition of 50 % CdO-NiO/PSi nanocomposites. The average distribution of nanoparticles size was found to be 47 - 59 nm [25].

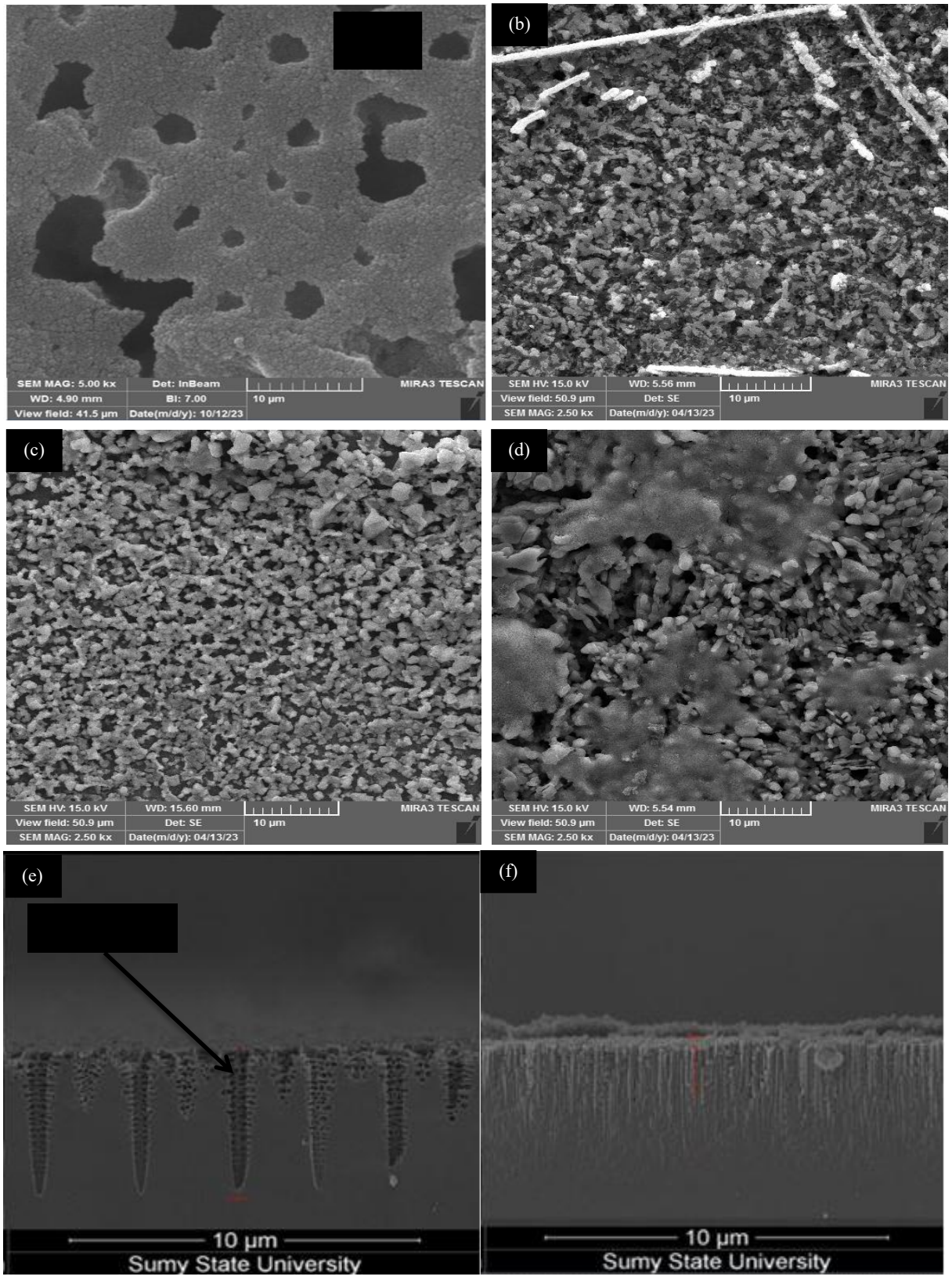

Figure 3 SEM images (a) PSi, (b) 25 % CdO-NiO/PSi, (c) 50 % CdO-NiO/PSi, (d) 75 % CdO-NiO/PSi, (e) Cross section PSi and (f) Cross section of 50 % CdO-NiO/PSi.

EDX analysis

Figure 4 reveals the EDX analysis spectrum of 75 % CdO-NiO/PSi nanostructures. The results indicate that the prepared samples have a good performance and homogenously. The analysis of elements C, O, Ni and Cd was presented as **Table 2**. The data confirm increasing of surface area of porous silicon, which can be characterized for numerous fields such as optoelectronic and biological applications [26].

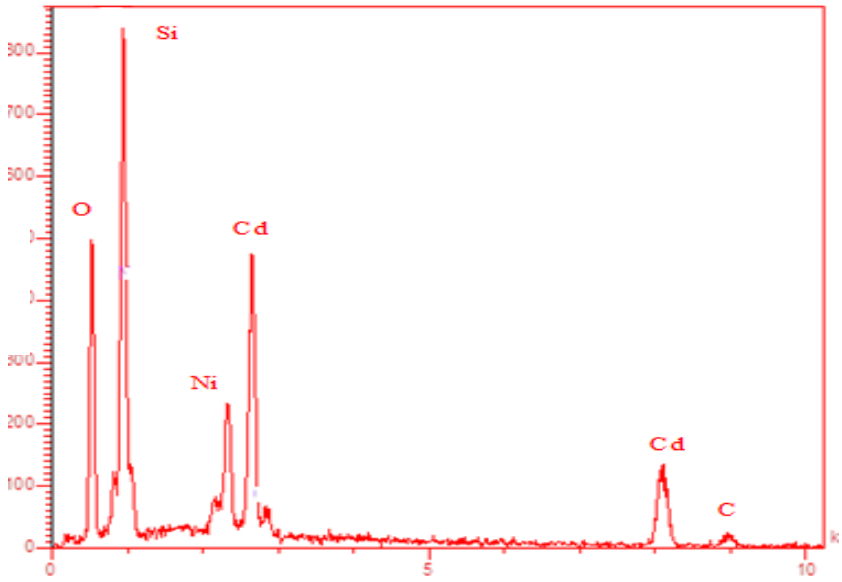

Figure 4 EDS analysis of 75 % CdO-NiO/PSi nanocomposites.

Table 2 Data of 75 % CdO-NiO/PSi nanocomposites.

Element	W%	Atomic%
O	20.62	14.26
Si	30.7	29.16
Cd	28.43	23.13
Ni	18.21	22.06
C	2.85	11.39
Totals	100	

Current-voltage characterization

The electrical properties of the NiO and CdO nanocomposites on porous silicon were carried out by using Keithley 4350 source Meter and WSE147s simulator. The current-voltage characterization was observed from –6 to 6 V at room temperature also a dual farnel LZ 20/2 power supply was used. The contact with the surface layer with respect to the Al electrode for all samples and shown in **Figure 5**. It was noted that the applied I-V measurements approach refers the presence of rectifying behavior of deposited samples [27]. Furthermore, the porous silicon substrate has a high resistivity due to excess of holes at the top surface and the trapped carriers at the pore wall which will form a region of potential barrier, this region will affect by the current transport causing the decreasing of the conductivity [28]. Clearly, the resistivity of the device decreases with the mixture the proportion of CdO with NiO nanocomposites on porous silicon due to formation of energy levels near from conduction band. Thun, the generation of the charge carriers and absorbed photons will increase at the surface. In the

other word, increasing of the cadmium oxide composite will produce higher conductivity. Besides, the CdO percentage is a significant factor to enhance the electrical properties as **Table 3**. Our results are good agreement with the other data [29].

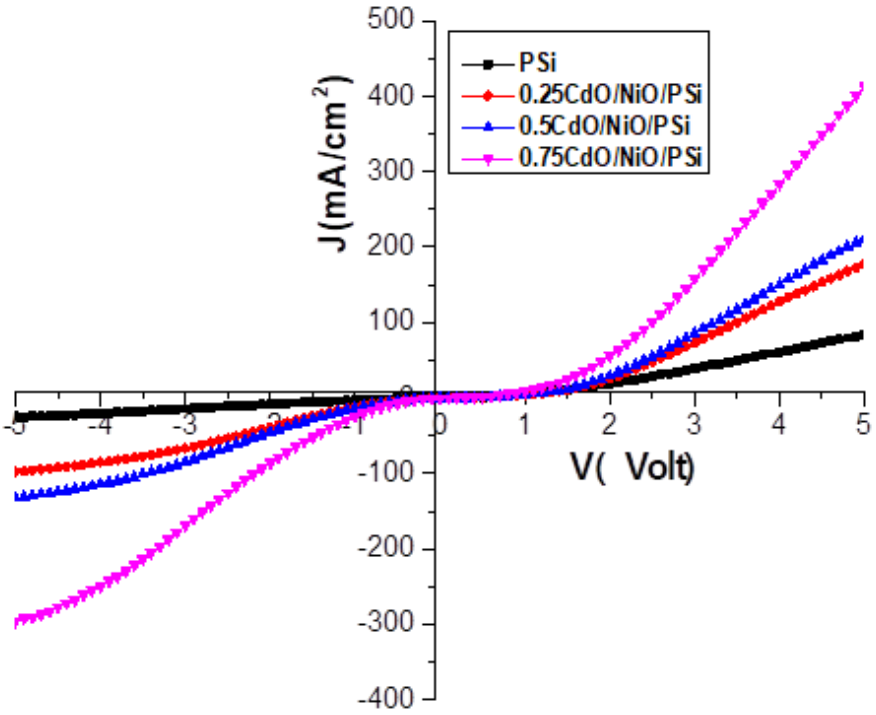

Figure 5 I-V measurements of CdO and NiO nanostructures deposited on porous silicon substrate.

Table 3 Values of carrier concentration, mobility and resistivity of CdO/NiO/PSi nanocomposites.

Sample	carrier concentration N (cm^{-3})	Mobility μ (cm^2/V.S)	(Ω.cm) ρ
PSi	6.8×10^{13}	0.75	5.7×10^{7}
0.25 CdO/NiO/PSi	13.25×10^{14}	9.62	4.53×10^{5}
0.5 CdO/NiO/PSi	7.82×10^{15}	13.74	6.77×10^{4}
0.75 CdO/NiO/PSi	1.92×10^{16}	19.82	1.77×10^{4}

Optical properties

Figure 6(a) shows the absorption spectra of CdO and NiO nanocomposites. The cadmium and nickel oxides were exhibited by UV-spectrophotometer. It can be seen the sharp peak of pure NiO NPs was found to be 355 nm of. Whereas the absorption peak of CdO NPs was observed at 450 nm. The absorption peak position was slight shifted in the red region with increasing of CdO content, the peak absorption edge was found to be 425, 427 and 432 nm for CdO at concentrations 25, 50 and 75 %, respectively, as **Figure 6(b)**. The optical band gap of the samples was determined using the relation [30,31]:

$$\alpha h\nu = A(h\nu - Eg)^{n} \quad (6)$$

where *n* represents a constant depending on the optical transition, Eg refers to the energy band gap, the symbol A *is* constant and $h\upsilon$ symbolizes the photon energy. The results indicate that the energy gap decreases with increasing of CdO content due to structural modifications. Thus, the extra energy levels at edge of valence band were observed [32,33]. The band gap of

fresh NiO and CdO nanostructures was found to be 3.3 and 2.21 eV, respectively. Furthermore, the energy gap of the cadmium oxide was found to be 2.69, 2.64 and 2.55eV at concentrations 25, 50, 75 %, respectively, as **Figures 7(a) - 7(c)**.

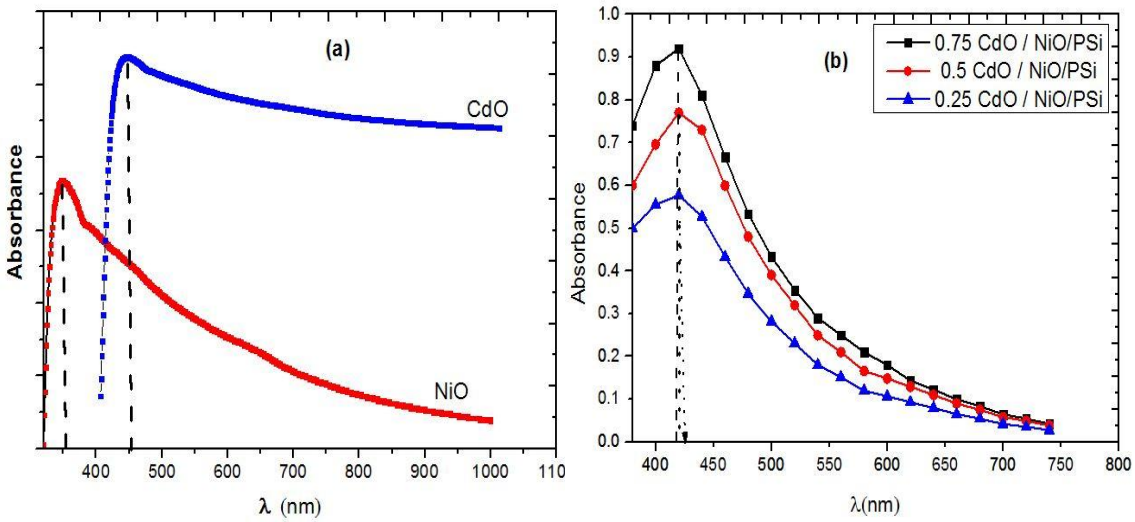

Figure 6 (a) Absorbance of CdO and NiO nanostructures and (b) Absorbance of CdO/NiO/Psi nanostructures at different ratio.

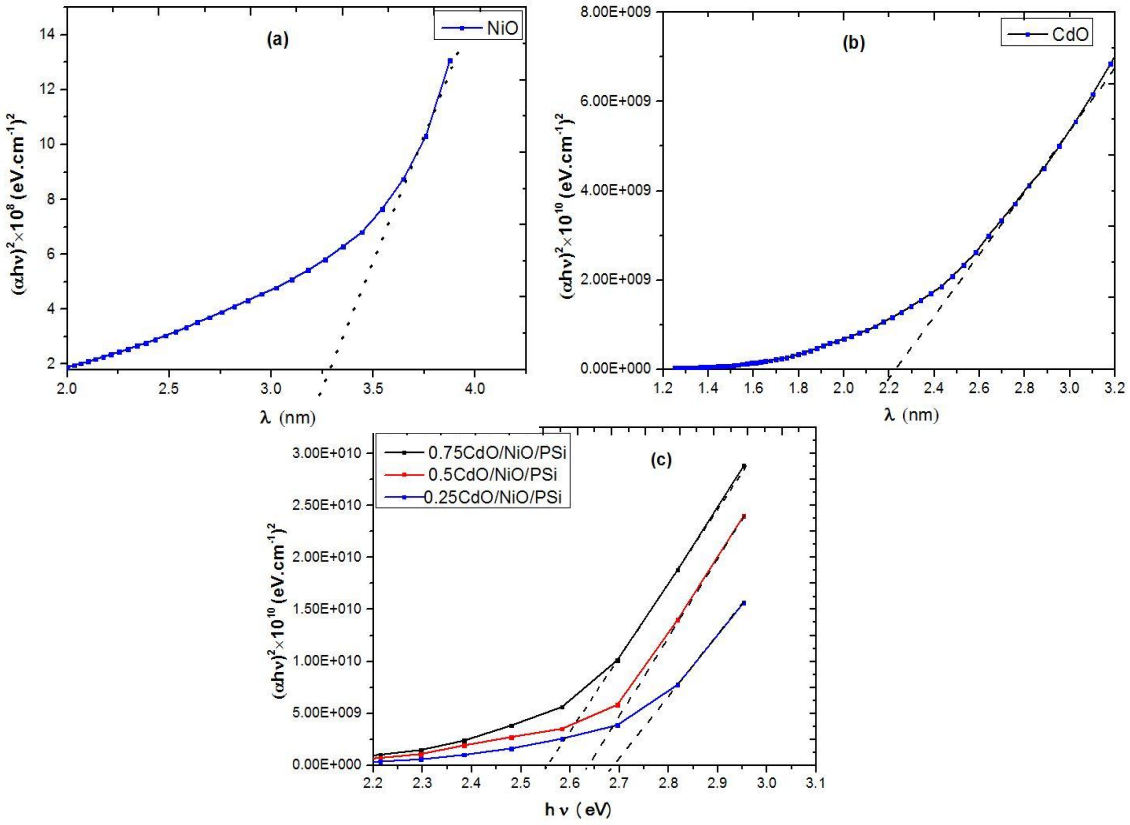

Figure 7 Calculation of energy gap (a) NiO, (b) CdO and (c) CdO/NiO/PSi nanocomposites at different ratio.

Influence of NPs on the viability of bacteria

A clear pattern emerged from the data of **Tables 4** and **5**, it can be noticed that the treatment of pathogenic and rhizobium bacteria with nanoparticles indicated no response at lower concentrations of 25 µg/mL. This is visibly illustrated in **Table 8**. However, when treating both pathogenic and non-pathogenic bacteria with a combination of Nickel nanoparticles and Cadmium nanoparticles, an insignificant impact on bacterial growth was noticed at the concentration of 25 µg/mL. On the contrary, **Table 6** indicates a stimulating effect on growth and no major effect on rhizobium bacteria. According to **Table 6**, it can be inferred that the best concentration was obtained when using a combination of Nickel nanoparticles, and Cadmium nanoparticles, with a colonization area of 23 cm. As for **Table 7**, it can be noticed that the influence was also obvious when using a mixture of nanoparticles at a concentration of 100 mg, although not as declared as the effect observed in **Table 7**. From **Table 7**, it is clear that the combination of nanoparticles has a significant impact on increasing the inhibition zone with *Pseudomonas aeruginosa* bacteria. The inhibition zone reached 21.9 mm at a concentration of 50 % CdO-NiO and 22.3 % at a concentration of 75 % CdO-NiO. These inhibition zones are considered large compared to other isolates of the bacteria. Similarly, *Rhizobium sp*. 2 bacteria exhibited a significant inhibition zone of 20.5 mm and 22.6 mm at 50 and 75 % of CdO-NiO, respectively. Our findings are consistent with the earlier study of [8,9,11]. Certainly, the use of nanoparticles in inhibiting bacterial growth has been a hot topic in recent years. Both cadmium and nickel nanoparticles have shown promising results in this area. From the available information, it appears that both cadmium and nickel have inhibitory effects on bacterial growth. Bacterial inhibition by nanoparticles is a complex process involving several mechanisms. A primary mechanism is the generation of reactive oxygen species (ROS), leading to oxidative stress and damage to bacterial cellular components like DNA, proteins, and lipids [32]. Nanoparticles can also disrupt bacterial cell membranes through direct interaction, increasing permeability and causing leakage of intracellular contents [33]. In addition, nanoparticles can release ions (eg AG+) that interfere with bacterial metabolism and enzyme function [34]. Some nanops also entered the bacterial cell and interacted with intracellular targets, contributed to cell death. These common effects make it difficult for bacteria to develop resistance to nanoplases [35]. However, cadmium shows more efficiency in killing nanopathy and inhibiting the growth of bacteria, these conclusions correspond to previous research [36]. Kadmium-nanopathy is effective in disrupting the development of bacteria due to their ability to damage the bacterial cell membrane and their ability to interfere with significant functions. A study published in the International Journal of Molecular Sciences found that the copper nanoplasts were E. coli can effectively prevent bacteria growth, making them a potential tool to handle bacterial infections [37]. On the other hand, cadmium nanopartanas worked to inhibit the growth of bacteria by producing reactive oxygen species, a type of free radicals that cause damage to bacterial cells. Both nickel and cadmium have been studied for their ability to prevent the development of harmful microorganisms. Researchers have examined nickel nanopathy for their antibacterial behavior and their ability to disrupt the adhesion and growth of dangerous microorganisms [38,39]. There is evidence that cadmium-nanopathy has an antibacterial effect as well and it has been studied to interfere with bacterial membrane, as well damage the bacterial cell membrane and their ability to prevent growth of the bacteria. The dosage, type of bacteria and size of nanosing is targeted special bacteria, among other factors, must also be kept in mind. **Figure 7** shows non-Gourd of Staphylococcus aurus (gram positive) and pseudomonus aeruginosa (gram negative) at a concentration of 750 mg/L with CdO-NiO/PSi and medium, if medium is supported if medium is supported. Petri Dish Treatment is on the right and control is on the left.

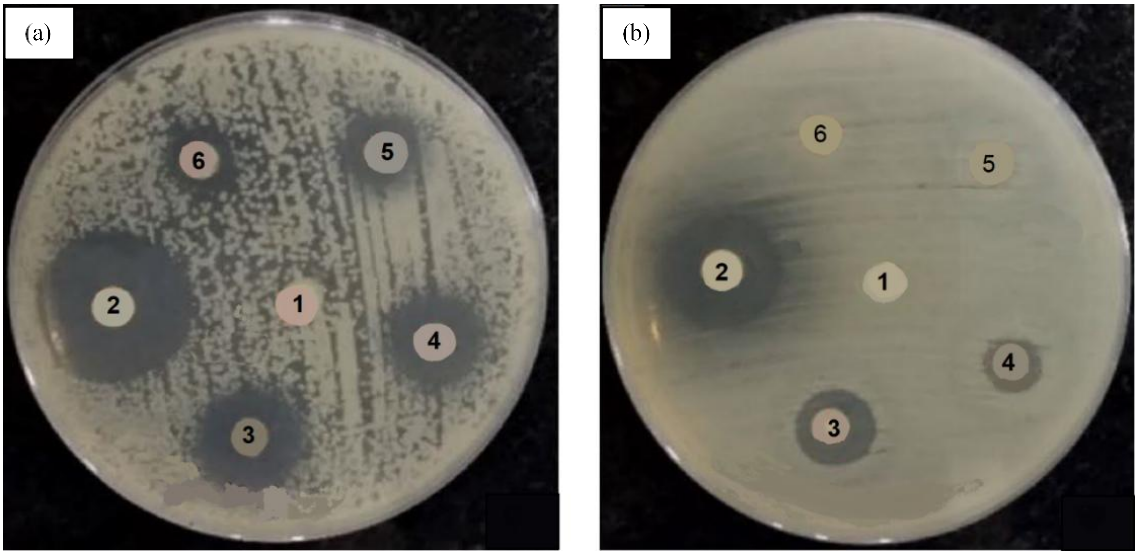

Figure 7 (a) The effect of nanoparticles on Gram-positive bacteria, showing big inhibition zones at intermediate concentrations and (b) Nanoparticle effects on Gram-negative bacteria, which showed relative resistance with smaller inhibition zones (e.g. disc no. 4 with a diameter of 12 - 14 mm).

Figure 7(a) shows the effect of nanoparticles on Gram-positive bacteria, where they showed special large inhibition zones at intermediate concentrations (e.g., disc #4 with a diameter of about 20 - 22 mm), indicating high sensitivity towards nanoparticles. As for **Figure 7(b)**, it represents the effect of nanoparticles on Gram-negative bacteria, which showed relative resistance with smaller inhibition zones (such as disc no. 4 with a diameter of about 12 - 14 mm). Gram-negative bacteria possess a complex outer membrane with lipopolysaccharides, acting as a barrier that limits nanocomposite penetration compared to Gram-positive bacteria's simpler peptidoglycan layer. This difference in cell wall structure affects ion diffusion, reactive oxygen species access, and physical interaction, resulting in varied susceptibility. Gram-negative bacteria's porins can also selectively restrict nanocomposite uptake, further contributing to their resistance. Gram-positive bacteria were counted as more affected by particles than Gram-negative, reflecting differences in cell wall composition between the 2 species. It is noted that intermediate concentrations were the most effective in both species, while the effect decreased at the highest concentrations probably due to saturation or toxic effects. The results indicate the possibility of using nanoparticles as an antibacterial agent taking into account the variation of response between species [40]. Nanocomposites combat bacteria in a number of ways: Their nanostructures physically obstruct bacterial attachment, growth, and replication; released ions harm cell membranes, causing leakage and death; and produced reactive oxygen species cause oxidative stress, impairing cellular functions. This combined strategy successfully inhibits bacterial growth and encourages cell death.

Table 4 The biological activity of the synergistic nanoparticles against different bacteria isolates, according to the rate of inhibition zone (mm), using the concentration of 25, 50, and 100 µg/mL.

Bacterial specimen	The mean diameter of the inhibition zone mm ± SD for samples that were treated with CdO			The mean diameter of the inhibition zone mm ± SD for samples that were treated with NiO		
	25 µg/mL CdO	50 µg/mL CdO	100 µg/mL CdO	25 µg/mL NiO	50 µg/mL NiO	100 µg/mL NiO
Control group	0.00	0.00	0.00	0.00	0.00	0.00
Staphylococcus aureus	08.1 ± 1.6	17.3 ± 1.5	18.5 ± 0.67	01.3 ± 0.68	15.3 ± 0.64	15.3 ± 1.6
Klebsiella pneumoniae	09.1 ± 0.64	11.53 ± 0.63	11.3 ± 0.68	02.3 ± 1.6	16.3 ± 1.1	15.4 ± 0.57
Pseudomonas aeruginosa	01.7 ± 0.7	15.73 ± 0.8	14.3 ± 1.37	05.3 ± 0.25	14.3 ± 0.51	17.3 ± 0.48
Bacillus subtilis	02.9 ± 1.33	16.3 ± 1.33	13.9 ± 0.30	09.3 ± 0.73	13.9 ± 0.6	16.3 ± 1.6
Rhizobium sp 1	02.63 ± 0.61	08.3 ± 0.47	15.3 ± 0.29	06.3 ± 1.6	13.2 ± 1.34	17.3 ± 0.63
Rhizobium sp 2	03.23 ± 0.68	15.36 ± 0.69	16.3 ± 1.6	09.3 ± 0.63	11.3 ± 0.63	16.22 ± 0.38
Rhizobium sp 3	02.3 ± 1.6	16.3 ± 1.1	16.3 ± 0.57	97.3 ± 0.7	14.5 ± 0.8	18.37 ± 1.34
Rhizobium sp 4	04.3 ± 0.55	16.63 ± 0.51	15.3 ± 0.48	13.2 ± 1.13	13.2 ± 1.35	17.53 ± 0.78

Table 5 The biological activity of the synergistic nanoparticles against different bacteria isolates, according to the rate of inhibition zone (mm), using concentration 25 µg/mL.

Bacterial specimen	Mean diameter of inhibition zone mm ± SD		
	25 % CdO	50 % CdO	75 % CdO
Control group	0.00	0.00	0.00
Staphylococcus aureus	6.3 ± 1.6	16.3 ± 1.6	21.3 ± 0.63
Klebsiella pneumoniae	07.3 ± 0.28	22.8 ± 0.62	23.3 ± 0.28
Pseudomonas aeruginosa	09.89 ± 0.7	12.3 ± 0.7	22.3 ± 1.34
Bacillus subtilis	10.3 ± 1.33	15.3 ± 1.33	19.3 ± 0.63
Rhizobium sp 1	06.9 ± 0.61	16.5 ± 0.63	21.6 ± 0.18
Rhizobium sp 2	08.3 ± 0.64	17.13 ± 0.69	19.6 ± 3.6
Rhizobium sp 3	04.3 ± 1.6	18.3 ± 1.1	22.3 ± 0.57
Rhizobium sp 4	05.3 ± 0.55	19.9 ± 0.51	21.8 ± 0.48

Table 6 The biological activity of the TiO nanoparticles against different bacteria isolates, according to the rate of inhibition zone (mm), using a concentration of 50 µg/mL.

Bacterial specimen	Zone of inhibition (mm)		
	25 % CdO	**50 % CdO**	**75 % CdO**
Control group	0.00	0.00	0.00
Staphylococcus aureus	11.3 ± 0.63	22.3 ± 0.7	21.3 ± 0.66
Klebsiella pneumoniae	14.2 ± 0.7	18.3 ± 1.37	19.3 ± 1.39
Pseudomonas aeruginosa	13.9 ± 1.39	21.3 ± 0.92	21.1 ± 0.69
Bacillus subtilis	11.3 ± 0.63	19.3 ± 0.66	15.3 ± 1.60
Rhizobium sp 1	09.7 ± 0.69	18.2 ± 1.6	22.3 ± 1.22
Rhizobium sp 2	04.3 ± 1.23	19.3 ± 0.57	19.3 ± 0.54
Rhizobium sp 3	09.5 ± 0.57	17.3 ± 1.22	12.3 ± 2.48
Rhizobium sp 4	13.2 ± 1.24	19.6 ± 1.88	19.3 ± 0.89

Table 7 The biological activity of the synergistic nanoparticles against different bacteria isolates, according to the rate of inhibition zone (mm), using a concentration of 100 µg/mL.

Bacterial specimen	Zone of inhibition (mm)		
	25 % CdO	**50 % CdO**	**75 % CdO**
Control group	0.00	0.00	0.00
Staphylococcus aureus	17.3 ± 0.97	18.3 ± 0.98	15.3 ± 1.18
Klebsiella pneumoniae	13.9 ± 1.2	14.5 ± 1.6	19.3 ± 0.89
Pseudomonas aeruginosa	16.3 ± 1.33	21.9 ± 0.63	22.3 ± 0.63
Bacillus subtilis	21.2 ± 0.63	15.3 ± 0.68	15.3 ± 0.68
Rhizobium sp 1	15.3 ± 0.68	17.3 ± 1.5	18.4 ± 1.6
Rhizobium sp 2	15.8 ± 1.6	20.5 ± 0.56	22.6 ± 0.59
Rhizobium sp 3	19.3 ± 0.57	14.8 ± 0.48	13.9 ± 0.48
Rhizobium sp 4	16.3 ± 1.6	18.3 ± 0.57	21.4± 0.57

Conclusions

In summary, the spraying method employed in this work was successful in improving the performance of CdO-NiO/PSi nanocomposites. SEM images showed that the surface topography has homogeneously distributed and depending on the Cd^{+2} content. XRD illustrated that the cadmium and nickel oxides thin films on porous silicon have a polycrystalline cubic structure. The crystalline size decreases with increasing of CdO ions. The energy gap of the CdO-NiO thin films was changed from the values 2.69 - 2.55 eV at composites 25 to 75 % CdO, respectively. The carrier concentration and the electrical resistivity owing to mixture of the Cd^{2+} ions lattice with Ni^{2+} ions on porous silicon substrate were observed. Cadmium and nickel oxide nanocomposites were effectively synthesized in the study utilizing a mixture exchange procedure with different ratios. The

concentrations of 50 and 100 µg/mL for 50 and 75 % CdO-NiO nanocomposites showed the most notable impacts, according to the biological activity assessment. Additionally, it was discovered that the symbiotic bacteria grew more readily at lower quantities of the nanoparticle mixture, 25 µg/mL. These results imply that CdO-NiO nanocomposites can be optimized for improved biological activity and possible biotechnological uses at particular concentrations. Finally, the nanoparticle NiO-CdO were found to possess toxic effects over bacteria and microalgae.

Acknowledgments

The authors thank college of education for pure science, Mosul University, Iraq for their logistic support.

References

[1] S Garba and A Yakubu. Nickel Oxide (NiO) devices and applications: A review. *International Journal of Engineering Research and Technology* 2019; **8(4)**, 461-467.

[2] AAA Al-Mushki, AAA Ahmed, AM Abdulwahab, SAS Qaid, NS Alzayed, M Shahabuddin, JMA Abduljalil and FAA Saad. Effect of the molar ratio of (Ni^{2+} and Fe^{3+}) on the magnetic, optical and antibacterial properties of ternary metal oxide CdO-NiO-Fe_2O_3 nanocomposites. *Scientific Reports* 2023; **13(1)**, 9021.

[3] B Abbas, AU Ahmad, S Shabbir, M Shahid, T Ahmad, MH Braga, I Naz, F Ahmad, Z Farooq and H Anwar. Enhancing photocatalytic and antibacterial performance through compositional optimization of NiO-CdO heterogeneous nanocomposites. *Ceramics International* 2023; **49(21)**, 33525-33536.

[4] TA Aswad, TA Abbas and GG Ali. Effect of deposition time on optical properties of CuO thin film prepared by chemical bath deposition method. *Digest Journal of Nanomaterials and Biostructures* 2021; **16(3)**, 831-838.

[5] OA Alhamd, GG Ali and MSH Aljuboori. Study and characterization of copper and titanium oxides nanostructures for some molecular and biological applications. *Trends in Sciences* 2024; **21(4)**, 7402.

[6] GG Ali, MA Ahmed and AA Sulaiman. Structural properties of AuNPs/PSi nanostructure. *Digest Journal of Nanomaterials and Biostructures* 2022; **17(2)**, 473-480.

[7] D Bonardo, N Darsono, S Humaidi, A Imaduddin and NS Silalahi. Effect of calcination frequency on the thermoelectric properties of Ti doped $CuCrO_2$ by solid state method. *Journal of Metals, Materials and Minerals* 2023; **33(4)**, 1785.

[8] D Bonardo, NLW Septiani, E Estananto, S Suyatman, S Humaidi and B Yuliarto. Synthesis and characterization of WO_3 sensitive layers for NO_2 gas sensor application. *In*: Proceedings of the Engineering Physics International Conference 2021, Yogyakarta, Indonesia. 2023, p. 50012.

[9] YN Al-Douri, N Badi and CH Voon. Etching time effect on optical properties of porous silicon for solar cells fabrication. *Optik* 2017; **147**, 343-349.

[10] O Bisia, O Stefano and L Pavesi. Porous silicon: A quantum sponge structure for silicon-based optoelectronics surface. *Science Reports* 2000; **38(1-3)**, 1-126.

[11] T Kumeria, SJP McInnes, S Maher and A Santos. Porous silicon for drug delivery applications and theranostics: Recent advances, critical review and perspectives. *Expert Opinion on Drug Delivery* 2017; **14(12)**, 1407-1422.

[12] H Föll, J Carstensen, M Christopersen and G Hasse. New view of silicon electrochemistry. *Physica Status Solidi* 2000; **182(1)**, 7-16.

[13] AA Sulaiman, GG Ali and AI Thanon. Synthesis and study of ZnO thin films using CVD technique for waveguide sensor applications. *Journal of Nanostructures* 2022; **12(1)**, 1-11.

[14] X Yang, F Xi, X Chen, S Li, X Wan, W Ma, P Dong, J Duan and Y Chang. Porous silicon fabrication and surface cracking behavior research based on anodic electrochemical etching. *Fuel Cells* 2020; **21(1)**, 52-57.

[15] J Park, Y Yanagida and T Hatsuzawa. Fabrication of p-type porous silicon using double tank electrochemical cell with halogen and LED light sources. *Sensors and Actuators B: Chemical* 2016; **233**, 136-143.

[16] R Vercauteren, G Scheen, JP Raskin and LA Francis. Porous silicon membranes and their applications: Recent advances. *Sensors and Actuators A: Physical* 2021; **318**, 112486.

[17] K Karthik, S Dhanuskodi, C Gobinath, S Prabukumar and S Sivaramakrishnan. Nanostructured CdO-NiO composite for multifunctional applications. *Journal of Physics and Chemistry of Solids* 2018; **112**, 106-118.

[18] AA Ezhilarasi, JJ Vijaya, K Kaviyarasu, M Maaza, A Ayeshamariam and LJ Kennedy. Green synthesis of NiO nanoparticles using *Moringa oleifera* extract and their biomedical applications: Cytotoxicity effect of nanoparticles against HT-29 cancer cells. *Journal of Photochemistry and Photobiology B: Biology* 2016; **164**, 352-360.

[19] S Anitha, M Suganya, D Prabha, J Srivind, S Balamurugan and AR Balu. Synthesis and characterization of NiO-CdO composite materials towards photoconductive and antibacterial applications. *Materials Chemistry and Physics* 2018; **211(1)**, 88-96.

[20] PA Thomas, O Alhamd, G Iszkuło, M Dering and TA Mukassabi. Biological flora of the British Isles: *Aesculus hippocastanum*. *Journal of Ecology* 2019; **107(2)**, 992-1030.

[21] K Karthik, S Dhanuskodi, C Gobinath, S Prabukumar and S Sivaramakrishnan. Multifunctional properties of microwave assisted CdO-NiO-ZnO mixed metal oxide nanocomposite: Enhanced photocatalytic and antibacterial activities. *Journal of Materials Science: Materials in Electronics* 2018; **29**, 5459-5471.

[22] NB Hasan and MJ Mohammed. Structural and morphological studies of $(NiO)_{1-x}(CuO)_x$ thin films prepared by chemical spray paralysis technique. *International Letters of Chemistry, Physics and Astronomy* 2015; **58**, 102-112.

[23] OA Hammadi, MK Khalaf and FJ Kadhim. Fabrication of UV photodetector from nickel oxide nanoparticles deposited on silicon substrate by closed-field unbalanced dual magnetron sputtering techniques. *Optical and Quantum Electronics* 2015; **3(1)**, 134-142.

[24] J Xu, S Liu, Y Yang, J Li, C Tian, L Guo, S Zhang, Y Liu and Z Zhong. Preparation of porous silicon by electrochemical etching methods and its morphological and optical properties. *International Journal of Electrochemical Science* 2019; **14(6)**, 5188-5199.

[25] MS Mohammed and RA Shlaga. Morphological and optical properties of porous silicon. *Engineering and Technology Journal* 2019; **37(1)**, 17-20.

[26] A Murat, S Gao, L Wang, L Chai, S Abliz and A Yimit. Synthesis and characterization of cadmium ion-imprinted/natural sand composite and research on its adsorption properties. *Coating* 2023; **13(7)**, 1288.

[27] I Syahidi, E Prayogo, B Pratama, K Triyana, K Khairurrijal, H Susanto and R Suryana. Porous silicon fabrication on N-type Si (111) electrochemical anodization technique with HF: Methanol solution. *Materials Today: Proceedings* 2021; **44(3)**, 3430-3433.

[28] K Omar and KA Salman. Effects of electrochemical etching time on the performance of porous silicon solar cells on crystalline n-type (100) and (111). *Journal of Nano Research* 2017; **46**, 45-56.

[29] O Volovlikova, S Gavrilov and P Lazarenko. Influence of illumination on porous silicon formed by photo-assisted etching of p-type Si with a different doping level. *Micromachines* 2020; **11(2)**, 199.

[30] S Khafory, KA Addim and G Ali. Effect of concentrations ratios of NiO on the efficiency of solar cell for $(CdO)_{1-x}(NiO)_x$ thin films. *Iraqi Journal of Physics* 2017; **15(33)**, 63-70.

[31] EA Saverina, DY Zinchenko, SD Farafonova, AS Galushko, AA Novikov, MV Gorbachevskii, VP Ananikov, MP Egorov, VV Jouikov and MA Syroeshkin. Porous silicon preparation by electrochemical etching in ionic liquids. *ACS Sustainable Chemistry and Engineering* 2020; **8(27)**, 10259-10264.

[32] AAA Ahmed, AAA Al-Mushki, BA Al-Asbahi, AM Abdulwahab, JMA Abduljalil, FAA Saad, SMH Qaid, HM Ghaithan, WA Farooq and AEH Omar. Effect of ethylene glycol concentration on the structural and optical properties of multimetal oxide CdO-NiO-Fe_2O_3 nanocomposites for antibacterial activity. *Journal of Physics and Chemistry of Solids* 2021; **155**, 110113.

[33] M Singh, AK Mallick, M Banerjee and R Kumar. Loss of outer membrane integrity in Gram-negative bacteria by silver nanoparticles loaded with *Camellia sinensis* leaf phytochemicals: Plausible mechanism of bacterial cell disintegration. *Bulletin of Materials Science* 2016; **39**, 1871-1878.

[34] Z Xu, C Zhang, X Wang and D Liu. Release strategies of silver ions from materials for bacterial killing. *ACS Applied Bio Materials* 2021; **4(5)**, 3985-3999.

[35] UM Nayef, HT Hussein and AMA Hussien. Study of photoluminescence quenching in porous silicon layers that using for chemical solvents vapor sensor. *Optik* 2018; **172**, 1134-1139.

[36] YS Ocak, D Batibay and S Baturay. Optical and electrical properties of Ni-doped CdO thin films by ultrasonic spray pyrolysis. *Journal of Materials Science: Materials in Electronics* 2018; **29**, 17425-17431.

[37] N Hossain, MH Mobarak, MA Mimona, MA Islam, A Hossain, FT Zohura and MA Chowdhury. Advances and significances of nanoparticles in semiconductor applications - A review. *Results in Engineering* 2023; **19**, 101347.

[38] M Aftab, MZ Butt, D Ali, ZH Aftab, MU Tanveer and B Fayyaz. Investigation of antifungal response of NiO and copper-doped NiO thin films against *Aspergillus niger* and *Macrophomina phaseolina* fungi. *Environmental Science and Pollution Research* 2022; **29**, 3840-3852.

[39] M Suganya, R Baskaran, VS Nagarethinam and AR Balu. Photoconductive and antimicrobial properties of *Psidium guajava* leaf extract mediated green synthesized SnS_2-CdO and SnS_2-NiO nanocomposites. *International Journal of Nanoscience* 2021; **20(4)**, 2150034.

[40] AM Al-Jezbi. Synthesis and study of some physical properties of (CdO/NiO) nanocomposite via sol-gel method and their antibacterial activities. *Albaydha University Journal* 2022; **4(2)**, 998-1017.